Scientia Pharmaceutica

ÖSTERREICHISCHE PHARMAZEUTISCHE GESELLSCHAFT

MDPI

Article

Anti-Sporotrichotic Activity, Lambert-W Inhibition Kinetics and 3D Structural Characterization of *Sporothrix schenckii* Catalase as Target of Glucosinolates from *Moringa oleifera*

Erick Sierra-Campos [1,*], Mónica A. Valdez-Solana [1], Estela Ruiz-Baca [2], Erica K. Ventura-García [1], Claudia I. Avitia-Domínguez [3], Miguel Aguilera-Ortiz [1] and Alfredo Téllez-Valencia [3]

[1] Facultad de Ciencias Químicas GP, Universidad Juárez del Estado de Durango, Av. Artículo 123 S/N Fracc. Filadelfia, Gomez Palacio 35010, Mexico
[2] Facultad de Ciencias Químicas, Universidad Juárez del Estado de Durango, Av. Veterinaria s/n. Circuito Universitario Col. Valle del sur, Durango 34120, Mexico
[3] Facultad de Medicina y Nutrición, Universidad Juárez del Estado de Durango, Av. Universidad y Fanny Anitúa S/N, Durango 34000, Mexico
* Correspondence: ericksier@ujed.mx

Abstract: Most human fungal infections exhibit significant defensive oxidative stress responses, which contribute to their pathogenicity. An important component of these reactions is the activation of catalase for detoxification. To discover new antifungal chemicals, the antifungal activity of methanol extracts of *Moringa oleifera* from two commercial products (Akuanandi and Mas Lait) was investigated. The methanolic extracts' activity against *Sporothrix schenckii* was determined using an assay for minimum inhibitory concentration (MIC) and minimum lethal concentration (MLC). The MIC concentrations varied between 0.5 µg/mL and 8 µg/mL. Akuanandi extract had the lowest MIC (0.5 µg/mL) and MLC (1 µg/mL) values. *M. oleifera* methanolic extracts were tested for catalase inhibition. The Ki values of the *M. oleifera* extract against *S. schenckii* catalase (SsCAT) was found to be 0.7 µg/mL for MOE-AK and 0.08 µg/mL for MOE-ML. Catalase's 3D structure in SsCAT is unknown. The homology of SsCAT was modeled with an in silico study using a 3D structure from SWISS MODEL and validation the predicted 3D structure was carried out using PROCHECK and MolProbity. Docking simulations were used to analyze protein interactions using Pymol, PoseView, and PLIP. The results revealed that *M. oleifera* glucosinolates interacts with SsCAT. A molecular interaction analysis revealed two inhibitor compounds (glucosinalbin and glucomoringin) with high binding affinity to key allosteric-site residues. The binding energies revealed that glucosinalbin and glucomoringin bind with high affinity to SsCAT (docking energy values: −9.8 and −9.0 kcal/mol, respectively). The findings of this study suggest that glucosinolates derived from *M. oleifera* could be used instead of synthetic fungicides to control *S. schenckii* infections. We hope that the findings of this work will be valuable for developing and testing novel natural anti-sporothrix therapeutic agents in the future.

Keywords: catalase; *Sporothrix schenckii*; *Moringa oleifera*; glucosinolates

Citation: Sierra-Campos, E.; Valdez-Solana, M.A.; Ruiz-Baca, E.; Ventura-García, E.K.; Avitia-Domínguez, C.I.; Aguilera-Ortiz, M.; Téllez-Valencia, A. Anti-Sporotrichotic Activity, Lambert-W Inhibition Kinetics and 3D Structural Characterization of *Sporothrix schenckii* Catalase as Target of Glucosinolates from *Moringa oleifera*. *Sci. Pharm.* **2022**, *90*, 70. https://doi.org/10.3390/scipharm90040070

Academic Editor: William A. Donaldson

Received: 1 October 2022
Accepted: 2 November 2022
Published: 4 November 2022

1. Introduction

Sporothrix schenckii is an ascomycetous thermodimorphic fungus that has been recognized as the sole causative agent of sporotrichosis, a worldwide subcutaneous mycosis, for more than a century. However, based on its physiological and molecular aspects, it has been suggested that *S. schenckii* is a complex of different species. The human disease has a wide range of clinical presentations and can be classified into fixed cutaneous, lymphocutaneous, disseminated cutaneous, and extracutaneous sporotrichosis [1].

Sporotrichosis caused by *S. schenckii* occurs as a result of the ingestion of soil, plants, or organic matter contaminated with the fungus. Sporotrichosis typically presents as papules

or pustules that form ulcerated nodules that contain regional lymphatics. Sporotrichosis is classified into cutaneous, pulmonary, and disseminated forms, with the cutaneous type being the most common disease. Risk factors that increase the risk of disseminated disease include being immunocompromised and having chronic obstructive pulmonary disease, alcohol use disorders, and diabetes. A common precaution is to wear gloves and long sleeves when handling soil. The gold standard for sporotrichosis diagnosis is fungal culture. The first-line treatment is itraconazole [2]. However, itraconazole should not be used in pregnant patients. Amphotericin B can be used after 12 weeks of gestation, but this drug is reserved for disseminated and pulmonary forms of the disease, especially in immunocompromised patients [2].

Azoles inhibit the oxidases present in fungal cell membranes, which prevents the fungal cell wall from producing sterols (ergosterol). This incomplete synthesis renders the cells permeable. Echinocandins, on the other hand, inhibit the synthesis of a key polysaccharide (1,3-β-glucan) involved in cell wall construction, whereas polyenes bind directly to ergosterol and translocate across the cell membrane into the cell to form pores. The organelles then come out and cause cell death [3]. Topical antifungals treat fungal infections by working at different sites to target molecules, but they can cause a variety of symptoms at the application site, such as burning, redness, and some allergic reactions [4,5].

ROS play various roles in fungi, including signaling pathways during development and environmental reactions. Because of their high reactivity, ROS levels in fungi must be tightly managed to prevent cell death. ROS production and scavenging play significant roles in pathogen–host interactions on both sides. The so-called oxidative burst is launched on the host side following infection and is often characterized by localized ROS buildup, which is detrimental to both infection partners and is central to the hypersensitive response. As a result, pathogenic fungi must successfully scavenge host-derived ROS to survive and achieve virulence [6]. Hence, there has been great interest in the strategies adopted by *S. schenckii* to avoid oxidative killing via macrophages and neutrophils. During infection, pathogens encounter oxidative stress, which they can overcome via their antioxidant defense systems, such as the production of superoxide dismutase and catalase enzymes. [7]. Catalase from *S. schenckii* has been reported to protect fungi from hydrogen peroxide [8]. However, the inhibition of this enzyme could make *S. schenckii* susceptible to rapid killing by hydrogen peroxide. Therefore, catalase is a putative virulence factor for *S. schenckii* [9,10].

Many therapeutic herbs are being studied for their ability to combat drug-resistant *S. schenckii*. In this regard, the anti-fungal potentials of well-known medicinal plants such as *Moringa oleifera* have been investigated. *M. oleifera* is a medicinal plant that contains antifungal, antiviral, antibacterial, and antioxidant compounds. Because the leaves contain 200 bioactive molecules, *M. oleifera* extracts have the potential to control fungal diseases. Some of these compounds have been reported to have antifungal properties, particularly against dermatophytic fungi, thus providing a justification for the use of Moringa in folk medicine to treat skin and other infectious diseases [11]. In addition, ethanol extracts showed antifungal activities in vitro against dermatophytes such as *Trichophyton rubrum*, *Trichophyton mentagrophytes*, *Epidermophyton floccosum*, and *Microsporum canis* [12].

The Mexican market is full of a wide variety of pharmaceutical, dietary, and cosmetic products available to the public. Most *M. oleifera*-based products are available in our country as daily capsules or teas containing simple powdered leaves. In addition, the demand for pharmaceuticals, cosmetics, and food products is very high in the domestic and international markets, leading to aggressive competition among suppliers and manufacturers. We recently analyzed a variety of commercial *M. oleifera* leaf products to develop a phytochemical fingerprint and found that all products had the same fingerprint but differed significantly in the number of biomolecules they contained. The total content of bioactive compounds in the samples ranged from 591.5 to 966.1 mg/100 g dry weight, and the total antioxidant activity of the *M. oleifera* samples was in the following order: Mas Lait > De Font Quer > Akuanandi > Infusionate > Terbal. We can see that their therapeutic effects can vary widely [13].

However, to the best of our knowledge, the antifungal activity of *M. oleifera* against *Sporothrix* has not yet been studied. Therefore, the purpose of this study was to investigate the anti-fungal properties of *M. oleifera* leaves extract (MOE) against *S. schenckii*, which is known to cause sporotrichosis in México. The main aim of the current study was to investigate the inhibitory potential of two commercial products (Akuanandi and Mas Lait) against *S. schenckii* catalase via a target-based drug discovery approach based on *M. oleifera*'s antifungal properties (in vitro and in vivo).

2. Materials and Methods

2.1. Preparation of the Extract

The extract was prepared using 23 g of dry-ground sample (Akuanandi or Mas Lait) and 260 mL of 80% methanolic solution. This mixture was then run through an ultrasonic bath at 42 KHz (BRANSONIC 3510R-MTH, Branson Ultrasonics Corporation, Danbury, CT 06813-1961, USA) at room temperature for 2 h and then filtered through Whatman filter paper number 1 and centrifuged at 3500 rpm for 5 min. The final extract was concentrated on a rotary evaporator (BÜCHI R-210, BÜCHI Labortechnik AG, Postfach, CH-9230 Flawil, Switzerland), placed in a deep freezer for 24 h, and lyophilized to obtain a powdered extract that was kept at −80 °C.

2.2. Yeast Cells Culture and MIC

Yeast cells were grown in Brain Heart Infusion (BHI) broth at 37 °C with orbital shaking (150 rpm) for 7 days. Cells were harvested from the culture differentiated by >95% to a yeast-like morphology. In the experiment, each cell type was washed three times with Hanks' balanced salt solution, pH 7.4, and then counted in a Neubauer chamber. The viability of each cell sample was determined by counting the number of colony forming units (CFU) after 5 days of incubation at 37 °C on BHI agar plates.

Yeast suspensions (approximately 1×10^3 colony forming units per milliliter (CFUs/mL)) were prepared in BHI broth and were added to a 96-well microtiter plate. Serial dilutions of the *M. oleifera* extracts were prepared with the medium and added to the wells. The plate was incubated at 37 °C for 48 h, and then *S. schenckii* yeast growth on the well bottoms was visually observed to determine the minimum inhibitory concentration (MIC).

2.3. Catalase Activity

Briefly, the decrease in absorbance of a 5 mM solution of H_2O_2 in 50 mM phosphate buffer, pH 7.0, for 60 s was recorded at 240 nm with a DR5000 Hach UV-Vis spectrometer (Loveland, CO, USA). The extinction coefficient of 54 M^{-1} cm^{-1} was used to calculate the activity [14]. The reaction was initiated by the addition of 1 µL (containing 28 ± 5 µg of protein) of cell free-cytosolic fraction, and full progress curve runs were carried out over 1 min. The measurements for each group sample were carried out in triplicate.

2.4. Protein Determination

Protein concentration was estimated via Lowry's method [15], using bovine serum albumin fraction V (Sigma-Merck, Toluca, México) as the reference standard.

2.5. Kinetics Data Processing

Measurements of enzymatic reactions were used to characterize enzymes regarding their substrate affinities (*Km*) and maximal reaction rates (*Vm*). *Km* and *Vm* were determined by incubating the enzyme with varying concentrations of substrate; the results are usually plotted as a graph of reaction (v) against concentration of substrate [*S*] giving a hyperbolic curve. However, it is difficult to fit the best hyperbola through the experimental points and to determine *Vm* with any precision by estimating the limit of the hyperbola at an infinite substrate concentration. Therefore, the disadvantage of this approach is that during the measurement, substrate concentrations change continuously when close to *Km* and

influence the rate of the reaction, as is clear from the relationship between [S] and v in Equation (1):

$$(d[S])/dt = v = (Vm*[S])/(Km + [S]) \quad (1)$$

In addition, many measurements at different substrate concentrations are needed.

Recently, Goličnik and Bavec [16] presented a more direct method of determining the *Km* and *Vm* of paraoxonase 1 based on the Lambert W function:

$$[P]_t = [S]_0 - Km * \ln\left(\frac{x}{\ln(2.4 * \frac{x}{\ln(1+2.4*x)})}\right) - 0.45869 * \ln\left(2 * \frac{x}{\ln(1+2*x)}\right)$$

where

$$x = \frac{[S]_0}{Km} * \exp\left(\frac{[S]_0 - Vm * t}{Km}\right)$$

The exact solution to the Michaelis–Menten equation in terms of the Lambert W function is not available in standard curve-fitting tools and is unfamiliar to most researchers in the life sciences. However, modern computer software packages such as GraphPad Prism or Curveexpert professional permit the calculation of an estimate of the mean enzymatic kinetic parameters via this method with good accuracy and precision.

2.6. Preparation of Enzyme Structure

To understand the interactions of the catalase with the ligands, the 3D structure of the target enzyme needs to be elucidated. Although the CAT structure has not been experimentally proven, we subjected the protein sequence of *Sporotrix schenckii* (UniprotKB = A0A0F2M7I5) to homology modeling using Swiss-Model (https://swissmodel.expasy.org/) accessed on 23 November 2021. Two templates with maximum sequence identity and query coverage were used for better homology structure prediction (Template 1: PDB ID = 6rjn.1.A Catalase from Fungi at 2.3 Angstroms, query coverage = 90%, sequence identity 60.58% and Template 2: PDB ID = 1a4e.1.A Catalase from *Saccharomyces cerevisiae*, query coverage = 90%, sequence identity 58.58%). The multiple-sequence alignment of A0A0F2M7I5 and two templates was performed (data not shown). Different online servers were used for structure assessment, including the Swiss-Model structure assessment tool and the Ramachandran plot. A Yasara Minimization server was used for energy minimization.

2.7. Model Validation

The stereochemical quality of each model was evaluated by the online servers MolProbity and Procheck and an ERRAT plot that gives a measure of structural error for each residue in the protein. ProSA was employed to detect the native structure compatibility.

2.8. Catalytic Active Site Prediction

CASTp (Computed Atlas of Surface Topography of Proteins) was used to find the catalytic sites.

2.9. Preparation of Ligands

In this study, nine phytochemicals of *M. oleifera* were used as ligands, while one classical inhibitor (3-amino-triazol) was used as the standard. The smiles format was obtained from the PubChem (https://pubchem.ncbi.nlm.nih.gov/) accessed on 23 November 2021 and FooDB databases (https://foodb.ca/compounds) accessed on 20 August 2021. The conformational search was performed using the Cheminformatic tools and databases for Pharmacology (https://chemoinfo.ipmc.cnrs.fr/) accessed on 20 August 2021, and the most stable conformers were chosen and optimized [17].

2.10. Molecular Docking Simulation

Blind docking simulations of the optimized most stable conformers (ligands and standard) against the target enzyme (catalase) were conducted using Webina 1.0.3 (AutoDock

Vina Ported to WebAssembly) and CB-Dock (cavity-detection guided blind docking), and PoseView: ZBH: Universität Hamburg (https://proteins.plus/#poseview) accessed on 10 December 2021 and Protein–Ligand Interaction Profiler (https://plip-tool.biotec.tu-dresden.de/plip-web/plip/index) accessed on 10 December 2021 were used to determine the binding pocket, amino acids and all ligand interactions in the *S. schenckii* catalase [18].

3. Results

3.1. Antifungal Effect of M. oleifera Extract

The in vitro antifungal activity was determined by testing the MOE extracts (ML and AK) against the fungi *S. schenckii*. Additionally, the values of minimum inhibitory concentration (MIC), and minimum lethal concentration (MLC) were determined as described by [19]. Figure 1 shows that *S. schenckii* was found to be susceptive to the ethanolic extracts with MICs 0.5–8 µg/mL, and its growth was completely inhibited by the extracts, which showed that extract had great potential antifungal properties. At MOE-AK concentration of 0.5 µg/mL, this extract completely inhibited the yeast growth of *S. schenckii*. Meanwhile, 8 µg/mL of MOE-ML completely inhibited growth. This was similar to a previous report about an antifungal bioassay on *M. oleifera* crude extracts against *Botrytis cinerea*, which indicated better mycelial growth inhibition by methanol leaf extract (99%). The minimum inhibitory concentration (MIC) was 5 mg/mL with 100% spore germination inhibition, and the minimum fungicidal concentration (MFC) was 10 mg/mL with 98.10% mycelial growth inhibition using broth micro dilution and poisoned food techniques [20].

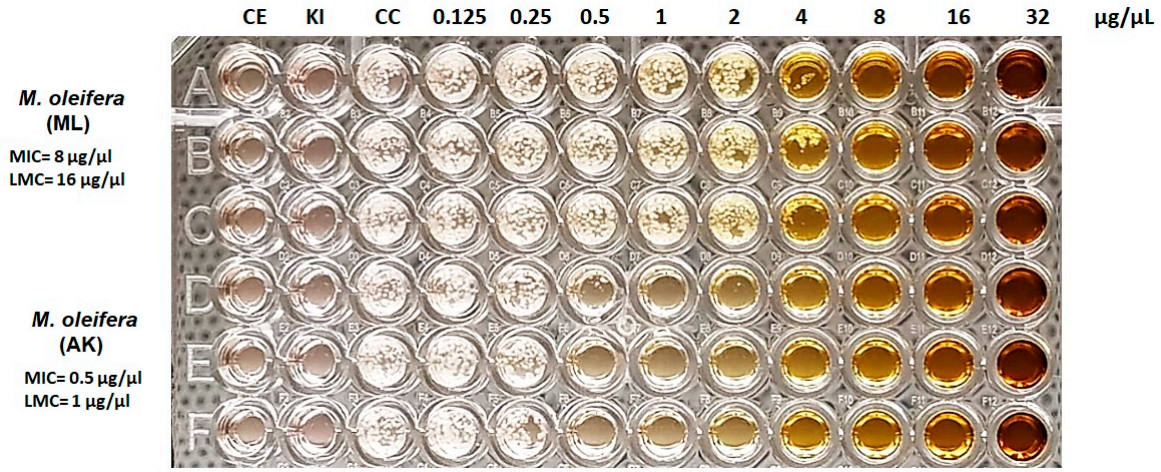

Figure 1. Determination of the minimum inhibitory concentration of extracts of *Moringa oleifera*. Growth of *S. schenckii* at 72 h in increasing concentrations of *Moringa oleifera* extracts. CE: sterility control, CKI: potassium iodide control, CC: growth control, MIC: minimum inhibitory concentration, LMC: minimum lethal concentration.

3.2. Effect of M. oleifera Leaves Extract on SsCAT Kinetic Parameters

We recently discovered that hydrogen peroxide induced *S. schenckii* catalase isoforms. As a result, it is plausible that *M. oleifera* extracts could influence *S. schenckii* development by suppressing catalase.

In this study, we explore the possible inhibitory role of *M. oleifera* on SsCAT. We found that both MOE-ML and MOE-AK extracts inhibited the catalase activity in a dose-dependent manner. However, the high antioxidant capacity makes it difficult to conduct enzymatic tests with the MOE-ML extract, and the points on the plot are widely spread. Despite the methodological problems, it was possible to obtain a good fit with the Lambert W function equation with a larger deviation than the control (Figure 2).

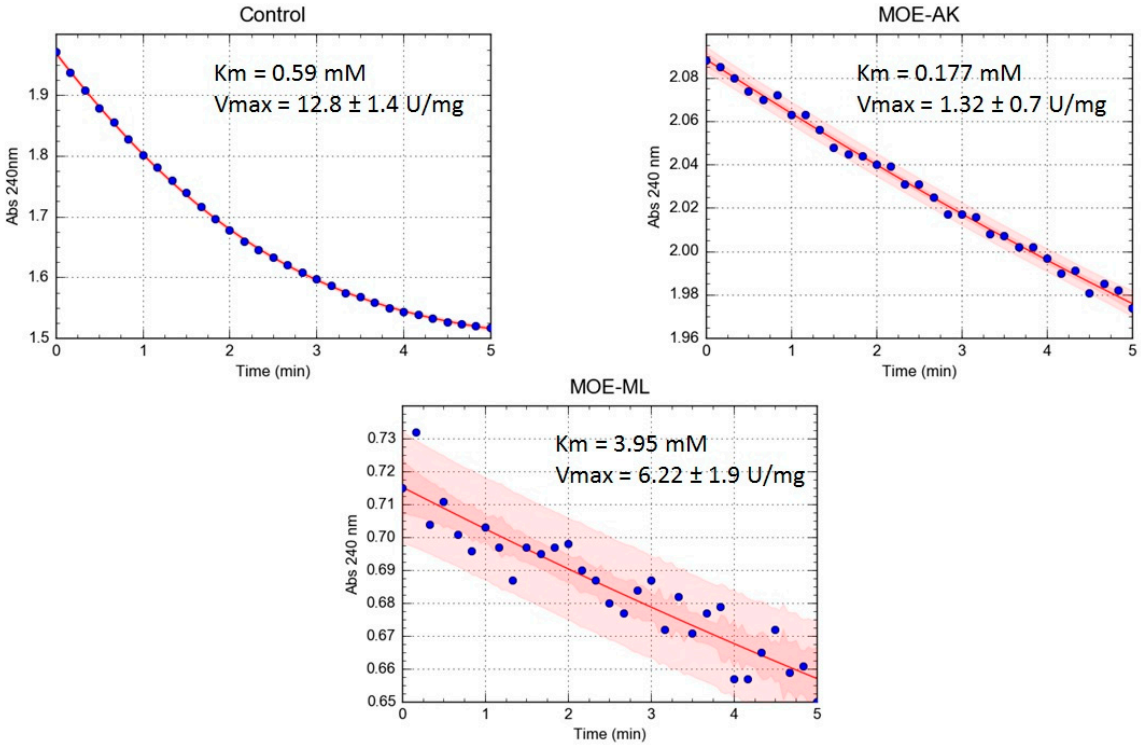

Figure 2. Calculation of *Km* and *Vm* from substrate concentration versus time plots. The image shows a representative trace of five repetitions for each rat of a different group.

We analyzed the Michaelis–Menten constant (*Km*) and the maximal velocity (*Vm*) of *S. schenckii*. The level of catalase in the cytosolic fraction was determined using progress curve kinetic analysis (Figure 2). A comparison of the kinetic data from the three groups revealed interesting results. With respect to the *Km* values, a significant decrease was observed in the SsCAT incubated with MOE-ML (*Km* = 3.95 mM) compared with the control (*Km* = 0. 59 mM). However, in the assay of SsCAT incubated with MOE-AK, the *Km* value diminished by nearly three times (*Km* = 0.177 mM), demonstrating that the MOE-AK substantially increased the affinity of the SsCAT for its substrate. On the other hand, the *Vm* value varied greatly between kinetics assays. In SsCAT incubated with MOE-ML, the *Vm* was one time lower than that of the control assay (*Vm* = 12.8 U/mg), whilst in the SsCAT incubated with MOE-AK, it diminished nine times (*Vm* = 1.32 U/mg). In addition, the *Vm*/*Km* ratio drastically decreased in enzymatic assays incubated with both extracts (1.57 and 7.45) compared with the control (21.69).

3.3. Homology Modeling

There are no experimental data or crystal structures of this SsCAT in the Protein Data Bank server. The homology modeling of protein structures has become a routine technique for generating 3D models of proteins when experimental structures are not available. A fully automated server with a user-friendly web interface such as Swiss-Model generates reliable models without the need to download complex software packages or large databases [21]. Since no crystal structure is available for catalase, we predicted catalase using Swiss-Model. This method has successfully predicted 3D structures of many enzymes [22].

The homologous proteins with known structures were explored for the template selection of target proteins in the PDB database updated on 15 June 2021 using the HHpred server. We found the crystal structure of catalase from *Kluyveromyces lactis* (PDB ID: 6RJR), whose structure was obtained by the expression system: Escherichia coli BL21, method: X-ray diffraction, Resolution: 1.90 Å, R-value free: 0.241, R-value work: 0.181 and R-value observed: 0.184. Hence, 6RJR showed maximum similarity with *S. schenckii* catalase and

was selected as the template with a sequence similarity of 98%, identities of 59%, E-value: 2.7×10^{-101} and QMEANDisCo Global 0.91 ± 0.05 (Figure 3). In addition, the average distance between the atoms (typically the backbone atoms) of a superimposed protein is measured as the root-mean-square deviation (RMSD). RMSD is commonly used to quantify the similarity of two or more protein structures. The lower the RMSD, the better the model compares to the target structure. Our 3D structural model exhibited a value of 0.235 for global RMSD.

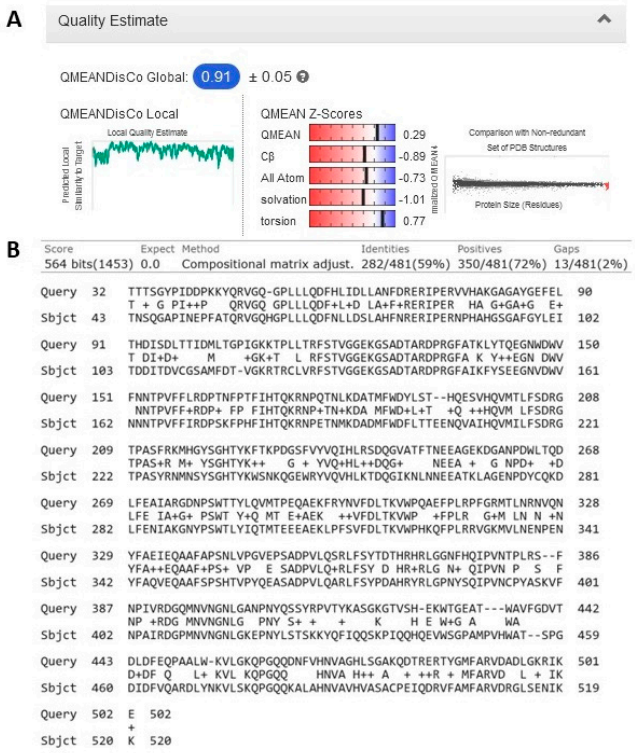

Figure 3. (**A**) Quality estimate of predicted structure of catalase from *S. schenckii*. (**B**) Amino acid alignment of from *S. schenckii* and the template *Kluyveromyces lactis* catalase.

The predicted 3D structure satisfied all the validation criteria on the basis of MolProbity and are illustrated in Table 1.

According to the Ramachandran plot analysis of the predicted structure, 90.4% of the residues' Φ/Ψ angles are in the most favored regions, 9.3% are in the additional allowed region, 0.2% are in the generously allowed region and 0% are in the disallowed region, as is shown in Figure 4A. Additionally, an overall value of 95.63 was observed for the quality factor, suggesting that the structure is a good quality model. Additionally, the ProSA-web server revealed that the model structure of *S. schenckii* catalase occupied the same region as that observed in the X-ray predicted native protein structure with a Z-score of −8.39. A negative Z-score is considered good, and it depends on the length of the protein. It was also observed that the overall residue energy of the *S. schenckii* catalase model was largely negative, except for a few peaks in some regions (Figure 4B). The overall quality of the final structure was further evaluated by Verify3D. The compatibility scores and the results for the final structure are presented in Figure 4C. The compatibility scores for all the residues in the developed model are above zero, and thus we inferred that the generated 3D model for catalase is reliable. The RMSD between the predicted structure and the template structure was found to be 0.235 Å, suggesting that the predicted 3D structure is an accurate model of *S. schenckii* catalase.

Table 1. 3D structural quality from SsCAT1.

All-Atom Contacts	Clashscore, All Atoms:	1		99th Percentile * (N = 1784, All Resolutions)
	Clashscore is the Number of Serious Steric Overlaps (>0.4 Å) per 1000 Atoms.			
Protein geometry	Poor rotamers	11	0.63%	Goal: <0.3%
	Favored rotamers	1669	95.81%	Goal: >98%
	Ramachandran outliers	0	0.00%	Goal: <0.05%
	Ramachandran favored	1932	96.75%	Goal: >98%
	Rama distribution Z-core	0.08 ± 0.19		Goal: abs (Z core) < 2
	MolProbity score^	1		100th percentile * (N = 27,675, 0–99 Å)
	Cb deviations > 0.25 Å	9	0.48%	Goal: 0
	Bad bonds:	0/16,525	0.00%	Goal: 0%
	Bad angles	126/22,448	0.56%	Goal: <0.1%
Peptide omegas	Cis prolines	4/140	2.86%	Expected: ≤1 per chain, or ≤5%
	Twisted peptides	3/2001	0.15%	Goal: 0
Low-resolution criteria	CaBLAM outliers	41	2.1%	Goal: <1.0%
	CA geometry outliers	14	0.70	Goal: <0.5%
Additional validations	Chiral volume outliers	0/2358		
	Waters with clashes	0/0	0.00%	See UnDowser table for details

In the two result columns, the left column gives the raw count and the right column gives the percentage. * The 100th percentile is the best among structures of comparable resolution; the 0th percentile is the worst. In terms of clashscores, the comparative set of structures was selected in 2004. for the MolProbity score, it was selected in 2006. The MolProbity score combines the clashscore, rotamer and Ramachandran evaluations in a single score, normalized to be on the same scale as X-Ray resolution.

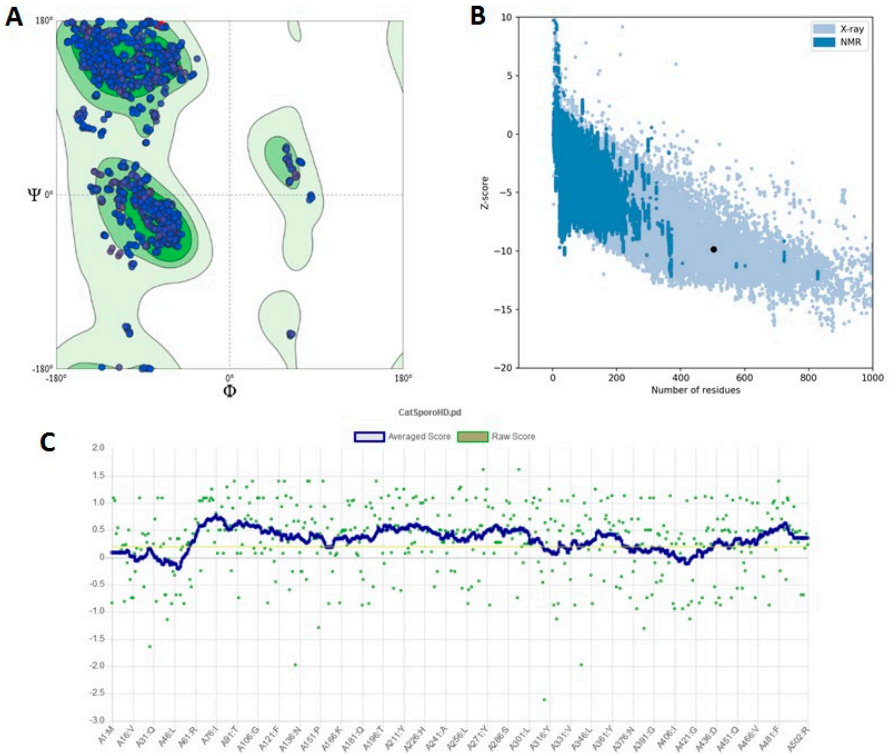

Figure 4. (**A**) Ramachandran plot of the predicted structure of *S. schenckii* catalase. The green regions in the plot indicate the most allowed regions, the additional allowed regions are shown in light green and the generously allowed regions are shown in gray shades. (**B**) Validation of the predicted catalase structure using the ProSA-web server. The Z-score in this plot is indicated by a dark black point. The structure is displayed with two distinguishable regions. The dark blue and light blue represent NMR and X-ray data, respectively. (**C**) Verify3D plot of the 3D catalase model with a 3D-1D averaged score (72.37%).

3.4. S. schenckii Catalase Features

The validated model was deposited in the Protein Modeling Database as PDBsum: cm95, and the Profunc server of EMBL-EBI was used to generate the wiring diagram (Figure 5) and the ProMotif documentation of the catalase.

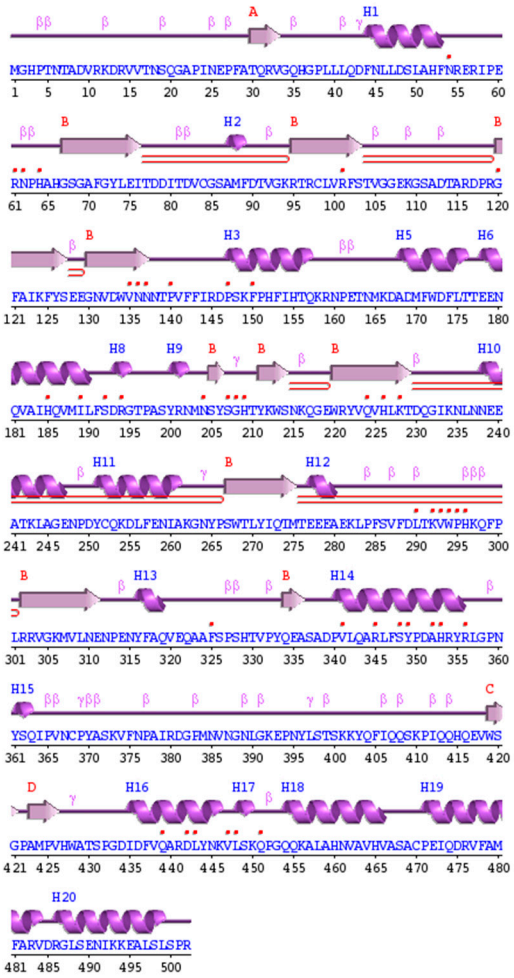

Figure 5. Wiring diagram of the predicted structure of *S. schenckii* catalase.

The analysis of the primary sequence of the catalase protein revealed a length of 510 amino acids with a molecular weight of 57,640 Da, gravy index = −0.68, aliphatic index = 61.39, theoretical isoelectric point = 6.42 and instability index II = 27.58, indicating that the protein is stable. The extinction coefficient was 79,300 M^{-1} cm^{-1}, which indicates the amount of light with a wavelength of 280 nm absorbed by the protein. The secondary structure of the catalase was assigned based on the locations of alpha helices in dark purple, beta-strands in light purple and coils in purple (Figure 5). The coils contributed the most (50% residues), followed by 18 α-helices (32% residues) and 13 strands (19% residues) in the protein.

The structure of *S. schenckii* catalase is not available in any structural databases. The 3D structure was predicted through the threading approach. Two predicted models were obtained with their corresponding QMEANDisCo Global scores. Model 1, which had a higher score (0.91 ± 0.05), was used for further analysis (Figure 2).

The dimensional structure of the modeled protein is presented as a cartoon representation created using PyMol (Figure 6). *S. schenckii* catalase has three domains with residues, including domain 1 (Chain A 380–438; Chain B 21–59), domain 2 (Chain B 60–152; Chain B 197–428), and domain 3 (Chain B 153–196, Chain B 429–502, Chain C 15–20).

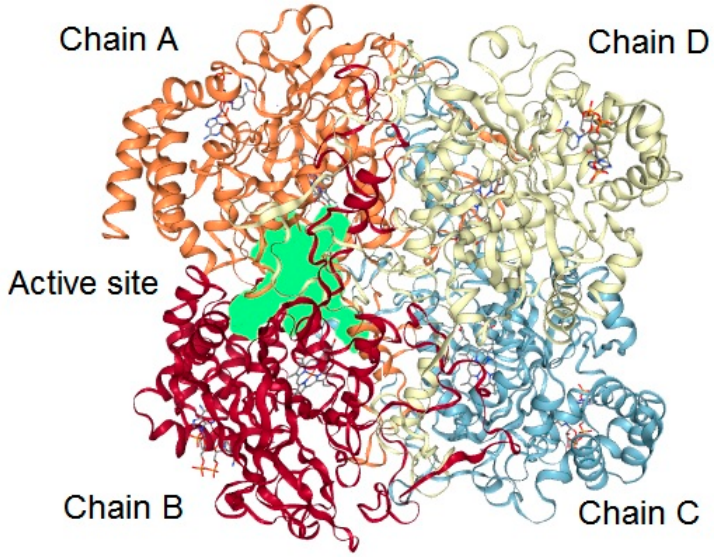

Figure 6. The structure and active site of *S. schenckii* catalase. The active site is surrounded by β-barrels, α-helices and loops. The active site of SsCAT1 is shown in light green.

The interaction of ligands (substrates or inhibitors) with the modeled protein was performed. CASTp was used to find the catalytic site (Figure 6). Its active site/binding region is located in the cleft between Chains A and B. The active site amino acids were in Chain A (Thr104, Val105, Gly106, Gly107, Glu108, Gly110, Ser111, Ala112, Thr114, Ala115, Arg116, Asp117, Pro118, Phe142, Phe143, Phe153, Ile154, Thr156, Gln157, Lys158, Arg159, Asn160, Thr163, Met165, Lys166, Asp167, Ala168, Asp169, Phe171, Leu190, Phe191, Thr196, Asn238, Ala241, Thr242, Ala245, Gly246, Asn248, Pro249, Asp250, Lys254, Glu258, Asn461, Val464, His465, Ser468 and Ala469) and Chain B (Thr104, Gly106, Gly107, Glu108, Gly110, Ser111, Ala112, Thr115, Arg116, Asp117, Pro118, Thr156, Gln157, Lys158, Arg159, Asn160, Thr163, Met165, Lys166, Asp167, Ala168, Asp169, Phe171, Leu190, Phe191, Thr196, Asn238, Ala241, Thr242, Ala 245, Gly246, Glu247, Asn248, Pro249, Asp250, Lys254, Glu258, Asn461, Val464, His465, Ser468 and Ala469).

3.5. Top Two Drug Candidates from Moringa oleifera

Natural products are important alternatives for the treatment of fungal infections because they contain well-known and described classes of molecules associated with antioxidant activities, in particular polyphenolic compounds. Molecular docking is a fast and efficient computational method for predicting the bioactive compounds of a specific protein or conversely for predicting the target proteins of a bioactive molecule [23].

Docking studies were performed to gain more insights into the binding mode of *M. oleifera* extract to SsCAT. The CB-Dock server was used to perform the automated molecular docking, and default parameters were used [24,25]. Five conformations were generated from the docking results. Conformation one showed the lowest binding energy and was considered for further analysis. Twelve candidates from *M. oleifera* were chosen to interact with catalase: 2-Methylpropylglucosinolate, glucotropaeolin, glucosinalbin, glucoputranjivin, glucoconringin, glucochlearin, glucomoringin, 4′-O-acetyl-4-(α-L-rhamnopyranosyloxy)-benzyl-GS, 4GBGS, 4′-O-acetyl-4-(α-L-glucopyranosyloxy)-benzyl-GS, 2-(α-L-rhamnopyranosyloxy)-benzyl-GS and isopropyl-GS. All compounds were evaluated, and glucosinalbin and glucomoringin were found to have the highest binding energy with SsCAT. It is worth noting that not all glucosinolates interact with the same cavity. The glucosinalbin binding site, for example, is deep within the cavity and not apparent from the surface, and it is formed by residues from all four subunits. Meanwhile, the glucomoringin binding site is present in a more superficial cavity, and only the C and D subunits are part of the cavity in this case (Figures 7A and 8A).

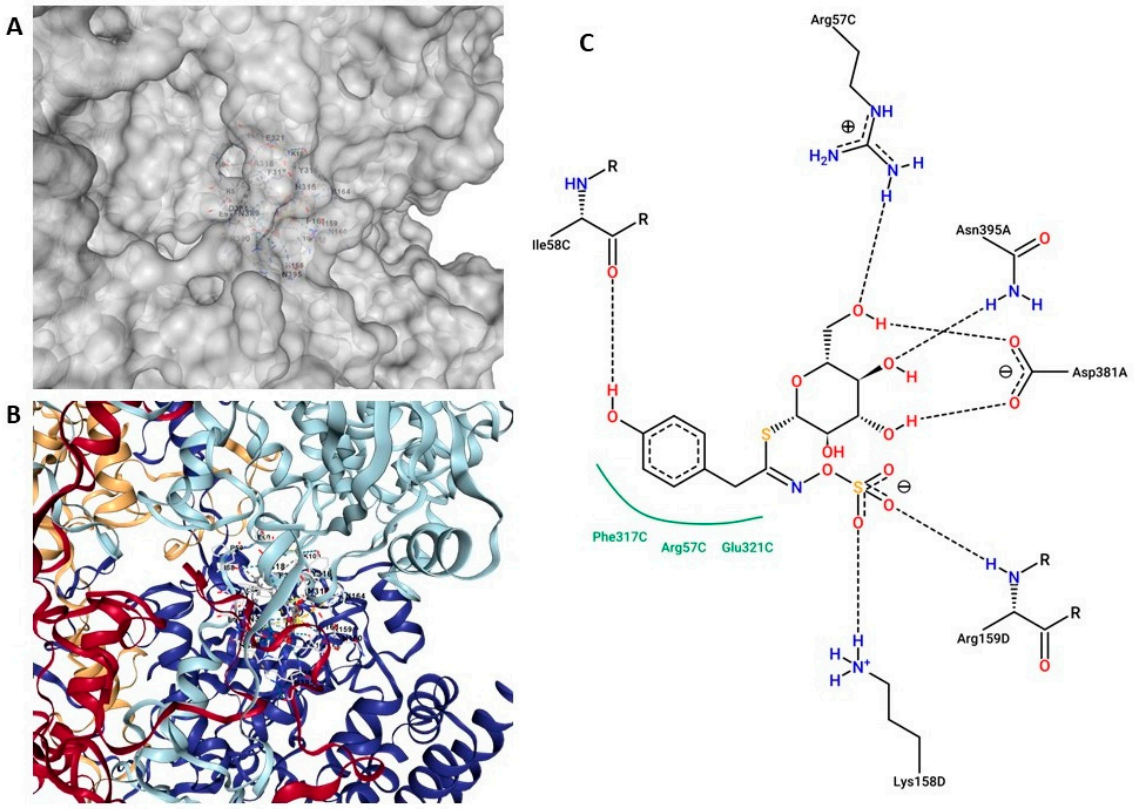

Figure 7. Docking results of the glucosinalbin–catalase complex. The binding site of the complex in space-filling view (**A**) and ribbon view (**B**), and the amino acids and chemical bonds involved in the interaction with catalase in a PoseView 2D interaction diagram (**C**).

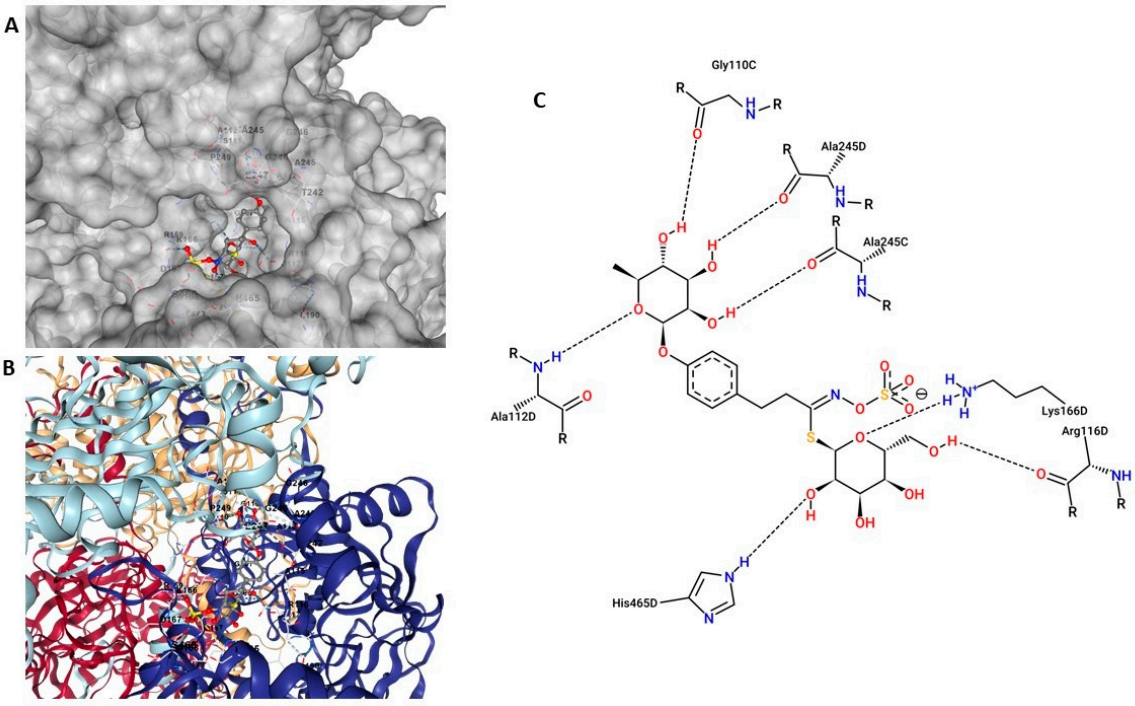

Figure 8. Docking results of the glucomoringin–catalase complex. The binding site of the complex in space-filling view (**A**) and ribbon view (**B**), and the amino acids and chemical bonds involved in the interaction with catalase in a PoseView 2D interaction diagram (**C**).

Glucosinalbin formed six hydrogen bonds with Ile58C, Arg57C, Asn395A, Asp381A, Arg159D and Lys158D and three hydrophobic interactions with Phe317C, Arg57C and Glu321C (Figure 7C). The p-hydroxybenzyl group of this compound was found to interact with Ile58C through hydrogen bonding and hydrophobic interactions. Further, there were three hydrogen bonds between β-d thioglucose and Asp381A, Asn395A and Arg57C. Finally, the sulfonated oxime group interacted with Lys158D and Arg159D through two hydrogen bonds. The glucosinalbin–catalase complex presented considerable binding affinity, with an energy value of −9.8 kcal/mol.

As is shown in Figure 8, the binding mode of glucomoringin docked to catalase showed seven H-bonding interactions with Ala112D, Ala245C, Gly110C, Ala245D, Lys166D, Asp117D and Gln157D. The β-d thioglucose group interacted with Gln157D, Asp117D and Lys 166D through hydrogen bonds. Further, the trihydroxy-6-(hydroxymethyl)oxan-2-yl group interacted with catalase through four hydrogen bonds with Gly110C, Ala112D, Ala245C and Ala 245D. The glucomoringin–catalase complex presented considerable binding affinity, with an energy value of −9.0 kcal/mol.

4. Discussion

Fungal infections are among the deadliest illnesses and are responsible for around 1.5 million fatalities worldwide each year [26]. The main reason why fungal diseases are becoming more dangerous is that they are being ignored by society [27]. Fungi respond to antifungal drugs by increasing their antioxidant stress response. Several studies have been conducted to investigate the role of key ROS-metabolizing enzymes such as catalases and superoxide dismutases in bacterial survival following antibiotic challenge. Antioxidant enzymes are also associated with antifungal potency. For example, sirtuin Hst1 deletion increases catalase activity and lowers multidrug sensitivity in *Candida glabrata* [28]. In a study, it was shown that exposure to a fungistatic dose of miconazole induces catalase activity in both *C. albicans* and *Saccharomyces cerevisiae* [29]. Evidence from the cited reports highlights the pivotal role that antioxidant enzymes play in mitigating the effects of various stress conditions.

Sporotrichosis is a subcutaneous mycosis that is particularly common in temperate and tropical Latin American countries, and it is has an annual incidence of >40,000. This illness is related to many vocations such as gardening, forestry, and fieldwork due to the presence of *Sporothrix schenckii* fungal components in vegetative matter [30]. The inescapable negative side effects of present treatments, as well as the increasing medication resistance among *Sporothrix* genera, necessitate the investigation of alternate therapeutic approaches. Because of their multi-targeting ability, medicinal herbs are gaining favor in the face of developing antimicrobial resistance.

Minami and Oliveira [31] identified no inhibitory antifungal action in an alcoholic extract of Bidens pilosa (Compositae), a plant widespread in America, Asia, and Africa, among the first reports of the search for plants with potential antifungal activity against *S. schenckii*. Fortunately, subsequent investigations have found satisfactory in vitro activity of other plant species examined in various extract forms, at various doses and with different techniques [32]. It is also worth mentioning that Valenzuela-Cota [33] showed that an antifungal fraction obtained from a *Jacquinia macrocarpa* plant (JmAF) showed a great ability to inhibit the spore viability of *Fusarium verticillioides*, and a great capacity to cause oxidative stress via the induction of ROS production. JmAF induced the highest ROS concentration and inhibited CAT and SOD activities.

Many in vitro and limited clinical studies have confirmed *M. oleifera*'s broad-spectrum antimicrobial (antibacterial, antifungal, antiviral, and antimycobacterial) properties, which may be attributed to its high polyphenol concentration and unidentified compounds [34]. In another study, the antifungal activity of *M. oleifera* ethanolic extracts was clearly shown against various fungi such as *Saccharomyces cerevisiae*, *Candida albicans* and *Candida tropicalis* [35]. *M. oleifera* ethanol extracts showed anti-fungal activities in vitro against dermatophytes such as *Trichophyton rubrum*, *Trichophyton mentagrophytes*, *Epidermophyton floccosum*

and *Microsporum canis* [12]. In addition, *M. oleifera* extracts showed antifungal activity against *Rizopus stolonifer* and *Microsporum gypsum*. An ethyl acetate extract was more active against *M. gypsum*, while *R. stolonifer* was more sensitive to a methanolic extract. The MIC ranged from 1.56 to 6.25 mg/mL for both extracts [11]. *Aspergillus flavus* was more susceptible to extracts with a high mean zone of inhibition, which was 12.80 ± 0.20 mm for *M. oleifera* methanolic extract and 11.40 ± 0.10 mm for *M. oleifera* ethanolic extract. For *Rhizopus stolonifera* the mean zone of inhibition was 9.66 ± 0.33 mm for a methanolic extract and 8.67 ± 0.10 mm for an ethanolic extract [36]. The antifungal activity *M. oleifera* ethanolic extract was clearly shown by the present study against various fungi such as *Saccharomyces cerevisiae*, *Candida albicans* and *Candida tropicalis* [35].

Despite the large number of studies reporting the antifungal activity of *M. oleifera*, there are no reports in the literature specifically describing the inhibition of *S. schenkii* by *M. oleifera* extract. Therefore, this study showed the anti-sporothrix effect of *M. oleifera* extract. The observed effects are thought to be caused by a wide variety of polyphenols and phenolic acids, as well as flavonoids, glucosinolates and possibly alkaloids. Previous results have suggested that the extract contained high levels of glucosinolates (GLSs) such as 4-(alpha-l-rhamnopyranosyloxy)-benzylglucosinolate and its three monoacetyl isomers, quercetin-3-O-glucoside and quercetin-3-O-(6′-malonyl-glucoside) but low levels of kaempferol-3-O-glucoside and kaempferol-3-O-(6′-malonyl-glucoside). The leaves of *M. oleifera* also contain 3-caffeoylquinic acid and 5-caffeoylquinic acid. *M. stenopetala* leaves contain rutin and quercetin 3-O-rhamnoglucoside (rutin). Proanthocyanidins and anthocyanins were not found in either species' tissues [37]. In addition, glucomoringin has been found to possess good antimicrobial activity against *Staphylococcus aureus* and *Enterococcus casseliflavus* [38].

Most fungal pathogens of humans display robust protective oxidative stress responses that contribute to their pathogenicity. The induction of enzymes that detoxify reactive oxygen species (ROS) is an essential component of these responses [6]. Our previous results demonstrate that oxidative stress induced by exogenous H_2O_2 leads to an altered lipid peroxidation, modifying CAT activity and the expression levels of the CAT genes, with CAT1 and CAT3 being the genes with the highest expression in response to an oxidizing agent [39]. These results show that CAT isoforms in *S. schenckii* can be regulated in response to oxidative stress and might help to control ROS homeostasis in fungus–host interactions.

We attempted to predict the 3D structure of CAT1 for *S. schenckii*. Because the structure of *S. schenckii* has not yet been resolved, we used Blastp to search for homologous sequences in the Protein Data Bank to build a 3D-model. The results showed several homologs of *S. schenckii* CAT1 sequence, and the CAT from *Kluyveromyces lactis* (PDB ID: 6RJR) was selected as a template based on its higher sequence identity and coverage and lower e-value. The reliability of the predicted CAT1 model was checked using various validation metrics, including Ramachandran plots, Z-scores and normalized qualitative model energy analysis scores. In addition, we compared our model with four different three-dimensional models of *S. schenckii* catalases in the Alphafold protein structure database (https://alphafold.ebi.ac.uk/search/text/Sporothrix schenkii catalase) accessed on 23 November 2021). However, they all belong to a single component (monomer), and their length varies from a fragment (1–327 amino acids) to a monomer with lengths of 1–740 aa. As a result, this study adds to our understanding of catalase's tetrameric structure (Figure 6). These structural results correlate well with those reported for the structure of other catalases. It is known that yeast peroxisomal catalases are a type of monofunctional heme catalase, often referred to as a classical catalase. Many are dumbbell-shaped homo-tetrameric enzymes with molecular weights ranging from 200 to 340 kDa. The N-terminal arm, the β-barrel globular domain, the connecting domain (also known as the wrapping loop) and a C-terminal -helical globular domain compose the monomer structure. The classical catalase β-barrel consists of an anti-parallel eight-stranded β-barrel with at least six inserted α-helices. The heme group is positioned in the core of each subunit and is linked to the catalase surface through a continuous solvent channel. According to phylogenetic analyses, classical

catalase sequences can be further classified into three clades that may have resulted from at least two gene duplication events. *Kluyveromyces lactis* catalase is a small-subunit clade 3-type catalase with heme b as a prosthetic group and NADPH as a second cofactor. Their shared monomeric fold is made up of four unique structural elements: (1) the N-terminal arm, (2) the central domain, (3) the wrapping loop, and (4) the C-terminal domain. Each protomer's 67-residue N-terminal arm travels along the interface between the two opposing chains and comprises only one β-strand (which couples up with the opposite monomer's last β-strand, β12) and one α-helix (1). Between α1 and β2, the N-terminal arm also contains a distal histidine (His64) an important catalytic residue [40]. Because the heme and NADPH bind to residues that are identical to those reported for *K. lactis*, the SsCAT has all the structural features of a peroxisome catalase.

Further, various physicochemical properties of *S. schenckii* CAT1 were calculated using different prominent resources, and active site identification was achieved. Previous molecular docking results by CBdock showed that glucosinolates of *M. oleifera* possesses a very similar binding mode with CAT1. The top two compounds, namely glucomoringin and glucosinalbin, showed the least binding energy and highest binding affinity among all the scrutinized compounds. Post-docking analyses showed the following free energy changes of −9.0 and −9.8 Kcal/mol for glucomoringin and glucosinalbin, respectively, and interacted with similar amino acid residues. Common residues involving H-bond interactions include Lys and Arg (Figures 6 and 7). However, Phe, Arg and Glu were found to anchor additional hydrophobic contact in the docked CAT1 structure (Figure 7). It is interesting to note that the glucosinolate binding site is different from the catalytic site where the heme group is located, and this result agrees well with the kinetic pattern of MOE-AK since its inhibition turned out to have an uncompetitive component, while MOE-ML has a mixed inhibition component.

Although the composition and concentration of glucosinolates vary in different crop species, organs, cultivars, and stages of development, sometimes in response to both abiotic and biotic factors, initiatives to improve individual compounds have been successful, leading to improved crop types with both nutritional and pharmacological benefits [41]. However, both extracts obtained from two commercial items (Akuanandi and Mas Lait) were effective at inhibiting *Sporothrix schenckii* growth. Therefore, our findings suggest that targeting CAT1 may be a promising strategy for selectively killing *S. schenckii* yeast. This may help us to identify molecular bases in the search for new effective treatments for Sporotrichosis using *M. oleifera* leaf extracts.

5. Conclusions

We found that methanol extracts from *M. oleifera* had significant antifungal activity. In particular, MOE-AK had the lowest MIC (0.5 μg/mL). According to our findings, both studied *M. oleifera* extracts have potential antifungal properties for the treatment of diseases caused by *S. schenkii*. In this study, the binding energy of the *M. oleifera* compounds and *S. schenckii* catalase ranged from −9.8 to −9.0 kcal/mol, indicating that these compounds could interact with the enzyme. Our results identified the two best compounds (glucosinalbin and glucomoringin), which can be considered promising inhibitors against *S. schenckii* catalase. However, more research with the isolated enzyme is needed to confirm the binding location of each of the glucosinolates to the protein.

Author Contributions: Conceptualization, E.S.-C., M.A.V.-S., E.R.-B. and A.T.-V.; formal analysis, E.S.-C., E.K.V.-G. and M.A.V.-S.; investigation, M.A.V.-S., E.R.-B., E.K.V.-G. and E.S.-C.; methodology, C.I.A.-D., E.R.-B. and M.A.V.-S.; software, A.T.-V. and E.S.-C.; supervision, M.A.-O. and E.S.-C.; writing—original draft, E.S.-C., M.A.V.-S. and E.K.V.-G. All authors have read and agreed to the published version of the manuscript.

Funding: This research received no external funding.

Institutional Review Board Statement: Not applicable.

Informed Consent Statement: Not applicable.

Data Availability Statement: Not applicable.

Acknowledgments: The authors thank Iván Artemio Corral Guerrero for the technical support he provided.

Conflicts of Interest: The authors declare no conflict of interest.

References

1. Oliveira, M.M.E.; Almeida-Paes, R.; Gutierrez-Galhardo, M.C.; Zancope-Oliveira, R.M. Molecular Identification of the Sporothrix Schenckii Complex. *Rev. Iberoam. Micol.* **2014**, *31*, 2–6. [CrossRef] [PubMed]
2. Sizar, O.; Talati, R. Sporotrichosis (Sporothrix Schenckii). In *StatPearls*; StatPearls Publishing: Tampa, FL, USA, 2018.
3. Marek, C.L.; Timmons, S.R. Antimicrobials in Pediatric Dentistry. In *Pediatric Dentistry*; Elsevier: Amsterdam, The Netherlands, 2019; pp. 128–141.e1.
4. Girois, S.B.; Chapuis, F.; Decullier, E.; Revol, B.G.P. Erratum: Adverse Effects of Antifungal Therapies in Invasive Fungal Infections: Review and Meta-Analysis. *Eur. J. Clin. Microbiol. Infect. Dis.* **2006**, *25*, 138–149. [CrossRef] [PubMed]
5. Kaur, N.; Bains, A.; Kaushik, R.; Dhull, S.B.; Melinda, F.; Chawla, P. A Review on Antifungal Efficiency of Plant Extracts Entrenched Polysaccharide-Based Nanohydrogels. *Nutrients* **2021**, *13*, 2055. [CrossRef] [PubMed]
6. Remmele, C.W.; Luther, C.H.; Balkenhol, J.; Dandekar, T.; Müller, T.; Dittrich, M.T. Integrated Inference and Evaluation of Host–Fungi Interaction Networks. *Front. Microbiol.* **2015**, *6*, 764. [CrossRef] [PubMed]
7. Dantas, A.d.S.; Day, A.; Ikeh, M.; Kos, I.; Achan, B.; Quinn, J. Oxidative Stress Responses in the Human Fungal Pathogen, Candida Albicans. *Biomolecules* **2015**, *5*, 142. [CrossRef] [PubMed]
8. Kajiwara, H.; Saito, M.; Ohga, S.; Uenotsuchi, T.; Yoshida, S. Impaired Host Defense against Sporothrix Schenckii in Mice with Chronic Granulomatous Disease. *Infect. Immun.* **2004**, *72*, 5073–5079. [CrossRef]
9. Romero-Martinez, R.; Wheeler, M.; Guerrero-Plata, A.; Rico, G.; Torres-Guerrero, H. Biosynthesis and Functions of Melanin in Sporothrix Schenckii. *Rev. Iberoam. Micol.* **2000**, *68*, 3696–3703. [CrossRef]
10. Ruiz-Baca, E.; Leyva-Sánchez, H.; Calderón-Barraza, B.; Esquivel-Naranjo, U.; López-Romero, E.; López-Rodríguez, A.; Cuéllar-Cruz, M. Identification of Proteins in Sporothrixschenckiisensu Stricto in Response to Oxidative Stress Induced by Hydrogen Peroxide. *Rev. Iberoam. Micol.* **2019**, *36*, 17–23. [CrossRef]
11. Zaffer, M.; Ganie, S.A.; Gulia, S.S.; Yadav, S.S.; Singh, R.; Ganguly, S. Antifungal Efficacy of Moringa Oleifera Lam. *AJPCT* **2015**, *3*, 28–33.
12. Chuang, P.; Lee, C.; Chou, J.; Murugan, M.; Shieh, B.; Chen, H. Anti-Fungal Activity of Crude Extracts and Essential Oil of Moringa Oleifera Lam. *Bioresour. Technol.* **2007**, *98*, 232–236. [CrossRef]
13. Sierra-Campos, E.; Valdez-Solana, M.A.; Avitia-Domínguez, C.I.; Téllez-Valencia, A.; Meza-Velázquez, J.A.; Aguilera-Ortiz, M.; Escobar-Ramírez, A. Standarization Based on Chemical Markers of Moringa Oleifera Herbal Products Using Bioautography Assay, Thin Layer Chromatography and High Performance Liquid Chromatography-Diode Array Detector. *Malays. J. Anal. Sci.* **2020**, *24*, 449–463.
14. Aebi, H. Catalase in Vitro. In *Methods in Enzymology*; Elsevier: Amsterdam, The Netherlands, 1984; Volume 105, pp. 121–126, ISBN 0076-6879.
15. Lowry, O.H.; Rosebrough, N.J.; Farr, A.L.; Randall, R.J. Protein Measurement with the Folin Phenol Reagent. *J. Biol. Chem.* **1951**, *193*, 265–275. [CrossRef]
16. Goličnik, M.; Bavec, A. Evaluation of the Paraoxonase-1 Kinetic Parameters of the Lactonase Activity by Nonlinear Fit of Progress Curves. *J. Enzym. Inhib. Med. Chem.* **2020**, *35*, 261–264. [CrossRef] [PubMed]
17. Margoliash, E.; Novogrodsky, A.; Schejter, A. Irreversible Reaction of 3-Amino-1:2:4-Triazole and Related Inhibitors with the Protein of Catalase. *Biochem. J.* **1960**, *74*, 339–348. [CrossRef] [PubMed]
18. Schneidman-Duhovny, D.; Inbar, Y.; Nussinov, R.; Wolfson, H.J. PatchDock and SymmDock: Servers for Rigid and Symmetric Docking. *Nucleic Acids Res.* **2005**, *33*, W363-7. [CrossRef] [PubMed]
19. Navarro-Tapia, E.; Nana, R.K.; Querol, A.; Pérez-Torrado, R. Ethanol Cellular Defense Induce Unfolded Protein Response in Yeast. *Front. Microbiol.* **2016**, *7*, 189. [CrossRef] [PubMed]
20. Ahmadu, T.; Ahmad, K.; Ismail, S.I.; Rashed, O.; Asib, N.; Omar, D. Antifungal Efficacy of Moringa Oleifera Leaf and Seed Extracts against Botrytis Cinerea Causing Gray Mold Disease of Tomato (*Solanum lycopersicum* L.). *Braz. J. Biol.* **2021**, *81*, 1007–1022. [CrossRef]
21. Biasini, M.; Bienert, S.; Waterhouse, A.; Arnold, K.; Studer, G.; Schmidt, T.; Kiefer, F.; Cassarino, T.G.; Bertoni, M.; Bordoli, L.; et al. SWISS-MODEL: Modelling Protein Tertiary and Quaternary Structure Using Evolutionary Information. *Nucleic Acids Res.* **2014**, *42*, W252–W258. [CrossRef]
22. Waterhouse, A.; Bertoni, M.; Bienert, S.; Studer, G.; Tauriello, G.; Gumienny, R.; Heer, F.T.; de Beer, T.A.P.; Rempfer, C.; Bordoli, L.; et al. SWISS-MODEL: Homology Modelling of Protein Structures and Complexes. *Nucleic Acids Res.* **2018**, *46*, W296–W303. [CrossRef]
23. Lee, A.; Lee, K.; Kim, D. Using Reverse Docking for Target Identification and Its Applications for Drug Discovery. *Expert Opin. Drug Discov.* **2016**, *11*, 707–715. [CrossRef]

24. Kochnev, Y.; Hellemann, E.; Cassidy, K.C.; Durrant, J.D. Webina: An Open-Source Library and Web App That Runs AutoDock Vina Entirely in the Web Browser. *Bioinformatics* **2020**, *36*, 4513–4515. [CrossRef] [PubMed]
25. Liu, Y.; Grimm, M.; Dai, W.; Hou, M.; Xiao, Z.-X.; Cao, Y. CB-Dock: A Web Server for Cavity Detection-Guided Protein–Ligand Blind Docking. *Acta Pharmacol. Sin.* **2020**, *41*, 138–144. [CrossRef] [PubMed]
26. Firacative, C. Invasive Fungal Disease in Humans: Are We Aware of the Real Impact? *Mem. Inst. Oswaldo Cruz* **2020**, *115*, 1–9. [CrossRef] [PubMed]
27. Mellado, E.; Cuenca-Estrella, M.; Rodríguez-Tudela, J.L. Clinical Relevance of Mechanisms of Antifungal Drug Resistance in Filamentous Fungi. *Enferm. Infecc. Microbiol. Clin.* **2002**, *20*, 523–530. [CrossRef]
28. Orta-Zavalza, E.; Guerrero-Serrano, G.; Gutiérrez-Escobedo, G.; Cañas-Villamar, I.; Juárez-Cepeda, J.; Castaño, I.; De Las Peñas, A. Local Silencing Controls the Oxidative Stress Response and the Multidrug Resistance in Candida Glabrata. *Mol. Microbiol.* **2013**, *88*, 1135–1148. [CrossRef]
29. De Nollin, S.; Van Belle, H.; Goossens, F.; Thone, F.; Borgers, M. Cytochemical and Biochemical Studies of Yeasts After In Vitro Exposure to Miconazole. *Antimicrob. Agents Chemother.* **1977**, *11*, 500–513. [CrossRef]
30. Mesa-Arango, A.C.; del Rocío Reyes-Montes, M.; Pérez-Mejía, A.; Navarro-Barranco, H.; Souza, V.; Zúñiga, G.; Toriello, C. Phenotyping and Genotyping of Sporothrix Schenckii Isolates According to Geographic Origin and Clinical Form of Sporotrichosis. *J. Clin. Microbiol.* **2002**, *40*, 3004–3011. [CrossRef]
31. Minami, P.S.; Oliveira, F. de Atividade Antifúngica de Bidens Pilosa L. *Rev. Bras. Farmacogn.* **1986**, *1*, 118–122. [CrossRef]
32. Waller, S.B.; Madrid, I.M.; de Faria, R.O.; Cleff, M.B.; de Mello, J.R.B.; Meireles, M.C.A. Anti-*Sporothrix* Spp. Activity of Medicinal Plants. *Braz. J. Pharm. Sci.* **2016**, *52*, 221–237. [CrossRef]
33. Valenzuela-Cota, D.F.; Buitimea-Cantúa, G.V.; Plascencia-Jatomea, M.; Cinco-Moroyoqui, F.J.; Martínez-Higuera, A.A.; Rosas-Burgos, E.C. Inhibition of the Antioxidant Activity of Catalase and Superoxide Dismutase from Fusarium Verticillioides Exposed to a Jacquinia Macrocarpa Antifungal Fraction. *J. Environ. Sci. Heal. Part B* **2019**, *54*, 647–654. [CrossRef]
34. Fouad, E.A.; Abu Elnaga, A.S.M.; Kandil, M.M. Antibacterial Efficacy of Moringa Oleifera Leaf Extract against Pyogenic Bacteria Isolated from a Dromedary Camel (Camelus Dromedarius) Abscess. *Vet. World* **2019**, *12*, 802–808. [CrossRef] [PubMed]
35. Patel, P.; Patel, N.; Patel, D.; Desai, S.; Meshram, D. Phytochemical Analysis and Antifungal Activity of Moringa Oleifera. *Int. J. Pharm. Pharm. Sci.* **2014**, *6*, 144–147.
36. Suraka, B.; Ibrahim, D.; Suleman, K.; Usman, U.; Usman, S.I. Antifungal Activity of Moringa Oleifera Leaves Crude Extract against Aspergillus Flavus and Rhizopus Stolonifer. *Dutse J. Pure Appl. Sci.* **2022**, *7*. [CrossRef]
37. Bennett, R.N.; Mellon, F.A.; Foidl, N.; Pratt, J.H.; Dupont, M.S.; Perkins, L.; Kroon, P.A. Profiling Glucosinolates and Phenolics in Vegetative and Reproductive Tissues of the Multi-Purpose Trees *Moringa oleifera* L. (Horseradish Tree) and *Moringa stenopetala* L. *J. Agric. Food Chem.* **2003**, *51*, 3546–3553. [CrossRef] [PubMed]
38. Galuppo, M.; Nicola, G.; Iori, R.; Dell'Utri, P.; Bramanti, P.; Mazzon, E. Antibacterial Activity of Glucomoringin Bioactivated with Myrosinase against Two Important Pathogens Affecting the Health of Long-Term Patients in Hospitals. *Molecules* **2013**, *18*, 14340–14348. [CrossRef]
39. Román-Casiano, K.M.; Martínez-Rocha, A.L.; Romo-Lozano, Y.; López-Rodríguez, A.; Cervantes-García, D.; Sierra-Campos, E.; Cuéllar-Cruz, M.; Ruiz-Baca, E. Enzyme Activity and Expression of Catalases in Response to Oxidative Stress in Sporothrix Schenckii. *Microb. Pathog.* **2021**, *161*, 105270. [CrossRef]
40. Gómez, S.; Navas-Yuste, S.; Payne, A.M.; Rivera, W.; López-Estepa, M.; Brangbour, C.; Fullà, D.; Juanhuix, J.; Fernández, F.J.; Vega, M.C. Peroxisomal Catalases from the Yeasts Pichia Pastoris and Kluyveromyces Lactis as Models for Oxidative Damage in Higher Eukaryotes. *Free Radic. Biol. Med.* **2019**, *141*, 279–290. [CrossRef]
41. Maina, S.; Misinzo, G.; Bakari, G.; Kim, H.-Y. Human, Animal and Plant Health Benefits of Glucosinolates and Strategies for Enhanced Bioactivity: A Systematic Review. *Molecules* **2020**, *25*, 3682. [CrossRef]